International Journal of Heat and Fluid Flow 33 (2012) 131–146

Contents lists available at SciVerse ScienceDirect

International Journal of Heat and Fluid Flow

journal homepage: www.elsevier.com/locate/ijhff

Influences of boundary conditions on laminar natural convection in rectangular enclosures with differentially heated side walls

Osman Turan [a,b], Robert J. Poole [a], Nilanjan Chakraborty [c,*]

[a] School of Engineering, University of Liverpool, Brownlow Hill, Liverpool L69 3GH, UK
[b] Department of Mechanical Engineering, Karadeniz Technical University, Trabzon 61080, Turkey
[c] School of Mechanical and Systems Engineering, Newcastle University, Claremont Road, Newcastle-Upon-Tyne NE1 7RU, UK

ARTICLE INFO

Article history:
Received 14 April 2011
Received in revised form 26 October 2011
Accepted 28 October 2011
Available online 25 November 2011

Keywords:
Laminar natural convection
Nusselt number
Constant wall temperature
Constant wall heat flux
Computational fluid dynamics

ABSTRACT

In this study, two-dimensional steady-state simulations of laminar natural convection of Newtonian fluids in rectangular enclosures with differentially heated side walls have been conducted. Two Prandtl numbers $Pr = 0.71$ and 7.0 – typical values for air and water – and a range of different aspect ratios $AR(=H/L$ where H is the enclosure depth and L is the enclosure width) ranging from 1/8 to 8 for constant heat flux boundary conditions are investigated for Rayleigh numbers in the range 10^4–10^6. To demonstrate the difference between the aspect ratio effects between the constant wall temperature and constant wall heat flux boundary conditions, simulations have also been carried out for the same range of numerical values of Rayleigh number for the constant wall temperature boundary condition. It is found that the mean Nusselt number $\overline{Nu}$ increases with increasing values of Rayleigh number for both constant wall temperature and constant heat flux boundary conditions. The effects of aspect ratio AR have also been investigated in detail and it has been found that the effects of thermal convection (diffusion) strengthens (weakens) with increasing aspect ratio and *vice versa*, for a given set of nominal values of Rayleigh number and Prandtl number for both types of boundary conditions. In the case of constant wall temperature boundary condition, the mean Nusselt number increases up to a certain value of the aspect ratio AR_{max} but for $AR > AR_{max}$ the mean Nusselt number starts to decrease with increasing AR. In contrast, the mean Nusselt number is found to increase monotonically with increasing AR for the constant wall heat flux boundary condition in the range of values of aspect ratio, Rayleigh number and Prandtl number considered in this study. Detailed physical explanations are provided for the observed phenomenon. Suitable correlations are proposed for the mean Nusselt number $\overline{Nu}$ for both constant wall temperature and wall heat flux boundary conditions which are shown to satisfactorily capture the correct qualitative and quantitative behaviour of $\overline{Nu}$ for the range of Rayleigh number and aspect ratio considered here.

1. Introduction

Natural convection in rectangular enclosures filled with Newtonian fluids has been analysed extensively by several researchers and interested readers are referred to Ostrach (1988), Gebhart et al. (1988), Khalifa (2001) and Ganguli et al. (2009) for detailed reviews. Although several boundary conditions for this problem are possible, differentially heated vertical side walls is one of the most analysed configurations (e.g. deVahl Davis, 1983). Unless stated otherwise, to avoid unnecessary repetition, the remainder of this paper will deal with this configuration for different aspect ratios (i.e. $AR = H/L$, in which H is the enclosure depth and L is the enclosure width) for Newtonian fluids. It has been shown in several previous studies (e.g. Elder, 1965; Gill, 1966; Newell and Schmidt, 1970; Yin et al., 1978; Bejan, 1979; Elsherbiny et al., 1982; Lee and Korpela, 1983; Wakitani, 1996) that AR plays a major role in the natural convection process in this configuration. However, natural convection in rectangular enclosures is often studied separately for tall ($AR \gg 1$) and shallow ($AR \ll 1$) enclosures and the vertical side walls are usually subjected to constant temperatures. Based on an extensive experimental analysis of this problem for tall enclosures Elder (1965) identified three distinct regions; a region in the vicinity of the vertical side walls where the temperature gradients are nearly horizontal and largest, an interior region where vertical temperature gradients appear and an end region strongly influenced by the boundary conditions. For small values of Rayleigh number[1] (i.e. $Ra_{CWT} < 10^3$), the isotherms remain parallel to the

* Corresponding author.
E-mail addresses: osmanturan@ktu.edu.tr (O. Turan), robpoole@liv.ac.uk (R.J. Poole), nilanjan.chakraborty@ncl.ac.uk (N. Chakraborty).

[1] The definition of Rayleigh number Ra_{CWT} will be provided later in Section 2 of this paper.

0142-727X/$ - see front matter © 2011 Elsevier Inc. All rights reserved.
doi:10.1016/j.ijheatfluidflow.2011.10.009

Nomenclature

a	constant (–)
AR	aspect ratio ($AR = H/L$) (–)
c_A, c_B, c_C	correlation parameter (–)
c_p	specific heat at constant pressure (J/kg K)
c_1, c_2, c_3	correlation parameter (–)
C_B	correlation parameter (–)
e	relative error (–)
f_1, f_2, f_3, f_4	functions relating thermal and hydrodynamic boundary layers (–)
F	fraction determining the ratio of the hydrodynamic boundary layer thickness on horizontal surface to the height of the enclosure (–)
g	gravitational acceleration (m/s^2)
g_1, g_2	functions (–)
Gr_{CWT}	Grashof number for the constant wall temperature configuration (–)
Gr_{CWHF}	Grashof number for the constant wall heat flux configuration (–)
h	heat transfer coefficient (W/m^2 K)
H	height of the enclosure (m)
k	thermal conductivity (W/m K)
K	thermal gradient in horizontal direction (K/m)
L	length of the enclosure (m)
n	correlation parameter (–)
n_B (–)	exponent of aspect ratio for self similar variation of mean Nusselt number in the boundary-layer regime (–)
Nu	Nusselt number (–)
Nu_1	convective contribution to Nusselt number (–)
Nu_2	conduction contribution to Nusselt number (–)

Subscripts

c	core
cen	centre of the domain
$conv$	convection contribution
C	cold wall
CWHF	constant wall heat flux
CWT	constant wall temperature
$diff$	diffusion contribution
ext	extrapolated value
H	hot wall

Special characters

T^*	reference temperature (=T_C for CWT case and =T_{cen} for CWHF case) (K)
ΔT	difference between hot and cold wall temperature (=($T_H - T_C$)) (K)
ΔT_1	the temperature difference between the horizontal walls (K)
ΔT_{char}	characteristic temperature difference (K)
ΔT_{cond}	temperature difference between vertical walls for pure conduction (K)
$\overline{Nu}$	mean Nusselt number (–)
p	apparent order of accuracy (–)
P	pressure (N/m^2)
Pr	Prandtl number (–)
q	wall heat flux (W/m^2)
q_e,q_f	correlation parameters (–)
$\dot{Q}$	thermal energy flow rate evaluated using an energy-flux integral over any cross-section at a given height (W)
Ra_{CWT}	Rayleigh number for the constant wall temperature configuration (–)
Ra_{CWHF}	Rayleigh number for the constant wall heat flux configuration (–)
T	temperature (K)
u_i	ith velocity component (m/s)
U, V	dimensionless horizontal ($U = u_1 L/\alpha$) and vertical velocity ($V = u_2 L/\alpha$) (–)
ϑ	characteristic velocity in vertical direction (m/s)
x_i	coordinate in ith direction (m)
α	thermal diffusivity (m^2/s)
β	coefficient of thermal expansion (1/K)
δ_{ij}	Kronecker's delta (–)
δ, δ_{th}	hydrodynamic and thermal boundary layer thickness (m)
θ_{CWT}	dimensionless temperature, ($\theta_{CWT} = (T - T_{cen})/(T_H - T_C)$) (–)
θ_{CWHF} (–)	dimensionless temperature ($\theta_{CWHF} = (T - T_{cen})k/qL$) (–)
μ	dynamic viscosity (N s/m^2)
$\boldsymbol{\nu}$	kinematic viscosity (m^2/s)
ρ	density (kg/m^3)
$\tau_{ij}(\tau)$	stress tensor (Shear stress) (Pa)
φ	general primitive variable
ψ	stream function (m^2/s)
max	maximum value
ref	reference value
$wall$	wall value
$\Delta_{\min,cell}$	minimum cell distance (m)
r_x, r_y	grid expansion ratio in x_1 and x_2 directions (–)

vertical boundaries and heat transfer takes place primarily due to conduction. For $10^3 < Ra_{CWT} < 10^5$, large values of temperature gradients are confined to near wall regions and a temperature stratification with an almost uniform vertical temperature gradient is established at the core. Complex secondary and tertiary flows appear in the interior region for larger values of Ra_{CWT}. Gill (1966) and Newell and Schmidt (1970) used analytical and computational methods respectively, to analyse natural convection in tall enclosures for high values of Ra_{CWT} where most of the heat transfer takes place in the thermal boundary layer adjacent to the vertical side walls. Gill (1966) obtained an asymptotic solution for tall enclosures in the limit of very large values of Rayleigh number (i.e. $Ra_{CWT} \to \infty$) with finite values of AR by matching the conditions of the core flow with the top and bottom boundary layers. Bejan (1979) subsequently refined the analysis of Gill (1966) and proposed expressions for mean values of Nusselt number for tall enclosures which are in good agreement with experimental data (Elder, 1965). A number of papers have investigated natural convection in tall enclosures both experimentally (Yin et al., 1978; Elsherbiny et al., 1982; Wakitani, 1996) and numerically (Lee and Korpela, 1983; Le Quéré, 1990; Wakitani, 1997; Zhao et al., 1997; Frederick, 1999; Lartigue et al., 2000; Dong and Zhai, 2007; Ganguli et al., 2009) and interested readers are referred to Ganguli et al. (2009) and references therein for a more detailed discussion.

Cormack et al. (1974a) analytically analysed natural convection in shallow enclosures (i.e. $AR \ll 1$) under asymptotic conditions of $AR \to 0$ for constant values of Ra_{CWT} and identified two convection regimes, namely, the parallel-flow regime and boundary layer regime. In the parallel flow regime, two horizontal counter-currents appear in the central core and the horizontal temperature gradient remains uniform throughout the interior region with the isotherms parallel to the vertical walls. In contrast, in the boundary-layer regime the regions of high thermal gradients are confined in the boundary layers adjacent to the vertical walls and convection

currents within the enclosure play a key role in thermal transport. Based on their analysis (for $AR \sim 0.1$), an approximate criterion for the parallel-flow regime was proposed by Cormack et al. (1974a) in the following manner: $Ra_{CWT}^2 AR^9 \leqslant 10^5$. Subsequently Cormack et al. (1974b) numerically investigated the transition between parallel-flow and boundary-layer regimes for enclosures with aspect ratios AR ranging from 0.05 to 1 and the simulation results were compared with the predictions of the asymptotic analysis by Cormack et al. (1974a). Cormack et al. (1974b) demonstrated that the parallel-flow regime appears with decreasing AR (Ra_{CWT}) for a given value of Ra_{CWT} (AR) and the thermal boundary-layer structure transforms to a linear variation of temperature within the enclosure. However, the Nusselt number obtained from the numerical simulations (Cormack et al., 1974b) was found to be greater than predictions of the asymptotic theory (Cormack et al., 1974a) for high values of $Ra_{CWT}^2 AR^9$. Bejan and Tien (1978) developed a complete set of analytical results for the mean Nusselt numbers corresponding to the three different regimes of convection in rectangular enclosures (parallel-flow regime, intermediate flow regime and boundary-layer regime, which are discussed in Section 3 in detail) and it was demonstrated that their analysis satisfactorily predicts the mean Nusselt number obtained from numerical (Cormack et al., 1974b) and experimental (Imberger, 1974) studies. In a subsequent study Bejan (1980) demonstrated that expressions of mean Nusselt number proposed in Bejan (1979) and Bejan and Tien (1978) do not, in fact, yield the same numerical value for square enclosures (i.e. $AR = 1.0$). Bejan et al. (1981) established a limiting condition (i.e. $Ra_{CWT} > AR^{-7}$) for which convection begins to play an important role in thermal transport in enclosures with differentially heated side walls based on an experimental investigation involving water. All of these aforementioned studies have been carried out for the differentially heated vertical side walls subjected to constant wall temperatures. The effects of aspect ratio on natural convection of Newtonian fluids in differentially heated vertical side walls subjected to constant wall heat flux (instead of constant wall temperature) have not been addressed in the existing literature.

This paper aims to address the aforementioned deficit in the existing literature. In this respect the main objectives of this paper are as follows:

1. To demonstrate the difference between the aspect ratio effects on natural convection in rectangular enclosures with differentially heated vertical side walls for constant wall temperature (CWT) and constant wall heat flux (CWHF) boundary conditions.
2. To explain the physical differences in the aspect ratio dependence of mean Nusselt number between the CWT and CWHF boundary conditions.
3. To propose a correlation for mean Nusselt number for the CWHF configuration for the aspect ratio range $1/8 \leqslant AR \leqslant 8$.

In order to meet the above objectives two-dimensional steady-state simulations have been carried out for aspect ratio $1/8 \leqslant AR \leqslant 8$ in the Rayleigh number range 10^4–10^6 at Prandtl numbers $Pr = 0.71$ and 7.0. It has been shown by Turan et al. (2010) that the mean Nusselt number in a square enclosure (i.e. $AR = 1$) changes only marginally with an increase in Prandtl number in the Rayleigh number range considered here. Thus, the present simulations have been carried out for just two values of Prandtl number representing two common Newtonian fluids such as air ($Pr = 0.71$) and water ($Pr = 7$). However given the weak Pr dependence demonstrated in the square enclosure (Turan et al., 2010) it is likely the findings reported here will be applicable for fluids with $Pr \gg 7$.

The rest of the paper will be organised as follows. The necessary mathematical background and details concerning the numerical implementation will be provided in the next section of the paper. Following this, the simulation results will be presented and subsequently discussed. Finally the main results will be summarised and conclusions will be drawn.

2. Mathematical background

2.1. Non-dimensional numbers

The Rayleigh number represents the ratio of the strengths of thermal transports due to buoyancy to thermal conduction, which can be defined as follows for the CWHF boundary condition:

$$Ra_{CWHF} = \frac{\rho^2 c_p g \beta q L^4}{\mu k^2} = Gr_{CWHF} Pr \tag{1}$$

where Gr_{CWHF} is the Grashof number in the CWHF condition and Pr is the Prandtl number, which are defined as:

$$Gr_{CWHF} = \frac{\rho^2 g \beta q L^4}{\mu^2 k} \text{ and } Pr = \frac{\mu c_p}{k} \tag{2}$$

For the CWT configuration the Rayleigh and Grashof numbers are defined as:

$$Ra_{CWT} = \frac{\rho^2 c_p g \beta \Delta T L^3}{\mu k} = Gr_{CWT} Pr \text{ and } Gr_{CWT} = \frac{\rho^2 g \beta \Delta T L^3}{\mu^2} \tag{3}$$

The Grashof number provides the ratio of the strengths of buoyancy and viscous forces while Pr describes the ratio of the strengths of momentum diffusion to thermal diffusion. Alternatively, Pr can be taken to represent the ratio of the hydrodynamic boundary layer to thermal boundary layer thicknesses. Using dimensional analysis it is possible to show that the Nusselt number for the CWHF (CWT) configuration is given by $Nu = g_1(Ra_{CWHF}, Pr, AR)$ ($Nu = g_2(Ra_{CWT}, Pr, AR)$) where Nu is given by:

$$Nu = \frac{hL}{k} \tag{4}$$

where the heat transfer coefficient h is defined as:

$$h = \left| -k \frac{\partial T}{\partial x_1}\bigg|_{wf} \times \frac{1}{|T_{x=0} - T_{x=L}|} \right| = \left| \frac{q}{T_{x=0} - T_{x=L}} \right| \tag{5}$$

where subscript '*wf*' refers to the condition of the fluid in contact with the wall.

2.2. Governing equations

For the present study steady-state flow of an incompressible Newtonian fluid with constant temperature independent thermophysical properties (e.g. specific heat c_p, viscosity μ and thermal conductivity k) is considered. For incompressible Newtonian fluids the conservation equations for mass, momentum and energy under steady state can be written using tensor notation (i.e. $x_1 = x$ is the horizontal direction and $x_2 = y$ is the vertical direction) as:

Mass conservation equation

$$\frac{\partial u_i}{\partial x_i} = 0 \tag{6}$$

Momentum conservation equations

$$\rho u_j \frac{\partial u_i}{\partial x_j} = -\frac{\partial P}{\partial x_i} + \rho g \beta \delta_{i2} (T - T^*) + \mu \frac{\partial^2 u_i}{\partial x_j \partial x_j} \tag{7}$$

Energy conservation equation

$$\rho u_j c_p \frac{\partial T}{\partial x_j} = \frac{\partial}{\partial x_j} \left(k \frac{\partial T}{\partial x_j} \right) \tag{8}$$

where the temperature at the geometrical centre of the domain is taken to be the reference temperature T^* for evaluating the buoyancy term $\rho g\beta\delta_{i2}(T-T^*)$ in the momentum conservation equations for the CWHF configuration. For the CWT configuration, the cold wall temperature T_C serves as the reference temperature T^*. The Kronecker delta δ_{i2} ensures that the buoyancy term $\rho g\beta\delta_{i2}(T-T^*)$ remains operational only in the momentum equation for the vertical direction (i.e. x_2-direction). The left hand sides of Eqs. (6) and (7) indicate the advective transport of momentum and thermal energy respectively. The terms on the right hand side of Eq. (6) denote the effects of pressure, buoyancy and viscous forces respectively. The right hand side of Eq. (7) depicts the effects of thermal diffusion due to conduction. In the present study the governing equations are solved in non-dimensional form, which are provided in Appendix A.

2.3. Boundary conditions

The simulation domain is shown schematically in Fig. 1 where the two vertical walls of a rectangular enclosure are subjected to either constant wall heat flux or constant wall temperature, whereas the other boundaries are considered to be adiabatic (i.e. $\partial T/\partial x_2|_{x_2=0}=0$ and $\partial T/\partial x_2|_{x_2=H}=0$) in nature. The velocity components (i.e. $u_1 = u$ and $u_2 = v$) are identically zero on each boundary because of the no-slip condition and impenetrability of rigid boundaries. For the CWHF configuration, the heat fluxes for the hot and cold vertical walls are specified according to Fourier's law of heat conduction (i.e. $-k(\partial T/\partial x_1)|_{x_1=0}=q$ and $-k(\partial T/\partial x_1)|_{x_1=L}=q$). In contrast, for the CWT case, the temperatures for the cold and hot vertical walls are specified (i.e. $T(x_1=0)=T_H$ and $T(x_1=L)=T_C$). The temperature boundary conditions for the horizontal insulated boundaries are given by: $\partial T/\partial x_2 = 0$ at $x_2 = 0$ and $x_2 = H$. The non-dimensional forms of the above boundary conditions are provided in Appendix A for the sake of completeness.

2.4. Numerical implementation

A finite-volume code is used to solve the coupled conservation equations of mass, momentum and energy in non-dimensional form. A second-order central differencing scheme is used for the discretisation of the viscous and thermal diffusion terms in Eqs. (6) and (7) and a second-order up-wind scheme is used for the advective terms in Eqs. (6) and (7). Coupling of the pressure and velocity is achieved using the well-known SIMPLE (Semi-Implicit Method for Pressure-Linked Equations) algorithm (Patankar, 1980), which implicitly takes care of the divergence free nature of incompressible fluid flow (i.e. mass conservation for incompressible fluid: $\nabla\cdot\vec{u}=0$). The discretised equations for a grid point P can be summarised in the following manner: $a_P\phi_P=\sum a_{nb}\phi_{nb}+b_P$ where ϕ is the primitive variable in question and a_P and b_P are the discretisation coefficients at point P and subscript '*nb*' is used to refer to the grid points in the neighborhood of point P. The convergence criteria were set to 10^{-9} for all the relative (scaled) residuals R_ϕ which is defined as: $R_\phi=\sum_{Cell\cdot P}\left|\sum a_{nb}\phi_{nb}+b_P-a_P\phi_P\right|/\sum_{Cell\cdot P}|a_P\phi_P|$.

2.5. Grid independency results

The grid independence of the results has been assessed based on an analysis of five different non-uniform meshes M1 (40×40), M2 (80×80), M3 (160×160), M4 (80×160) and M5 (80×320) and the details of these grids are included in Table 1. For $AR\leqslant1$ (M1–M2–M3) and for $AR>1$ (M2–M4–M5) different meshes were used to assess the numerical uncertainty. For some representative simulations ($Ra_{CWHF}=10^6$ and $Pr=7$ for $AR=0.5$ and 4) the numerical uncertainty is quantified here using Richardson's extrapolation theory (Roache, 1997). For a primitive variable ϕ the Richardson's extrapolation value is given by: $\phi_{h=0}=\phi_1+(\phi_2-\phi_1)/(r^p-1)$ where ϕ_1 is obtained based on fine grid and ϕ_2 is the solution based on next level of coarse grid, r is the ratio between coarse to fine grid spacings and p is the theoretical order of accuracy. In this analysis the apparent order of accuracy p was taken to be 2. The numerical uncertainties for the mean Nusselt number $\overline{Nu}=\int_0^H Nudx_2/H$ and the maximum non-dimensional vertical velocity (V_{max}) magnitude on the horizontal mid-plane of the enclosure are presented in Table 2. As seen in Table 2, the maximum numerical uncertainty levels between meshes are at most less than 2% for $\overline{Nu}$ and V_{max} in both aspect ratio cases. Based on these uncertainties, mesh M2 was used for $AR\leqslant1$, mesh M4 used for $AR=2$ and mesh M5 was used for $AR=4$ and 8. Using these meshes it has been estimated that the $\overline{Nu}$ values reported here are accurate to within 0.1%. In addition to this grid-dependency study, the simulation results for square enclosures were compared with the benchmark data of deVahl Davis (1983) and the agreement between the results was found to be very good and entirely consistent with the aforementioned grid-dependency studies. Interested readers are referred to Table 3 of Turan et al. (2010) for further details on benchmarking of the square configuration case (i.e. $AR=1.0$) with CWT boundary condition. Moreover, the variation of $\overline{Nu}$ with AR for the CWT boundary condition are found to be in agreement with the data presented in Bejan (1980) (see Fig. 6 later in this paper), which also serves as a validation for the present simulations.

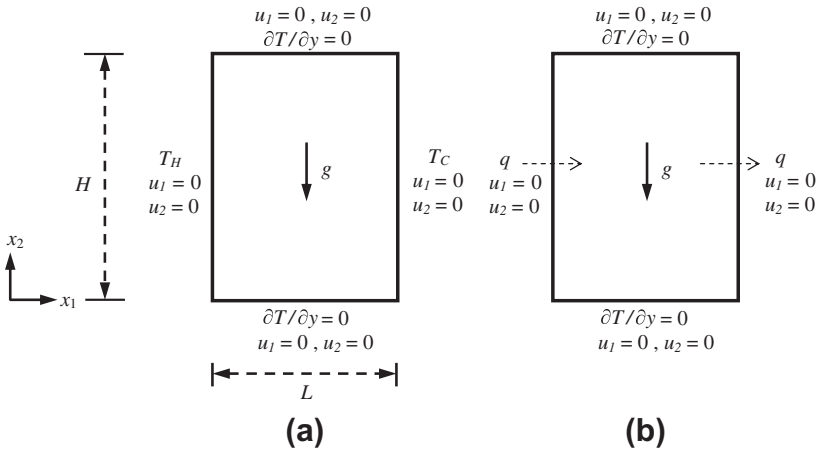

Fig. 1. Schematic diagram of the simulation domain.

Table 1
Non-dimensional minimum cell distances ($\Delta x_{min,\ cell}/L$, $\Delta y_{min,\ cell}/H$) and grid expansion ratios (r_x, r_y) values.

	Grid	M1 40 × 40	M2 80 × 80	M3 160 × 160
$AR = 0.125$	$\Delta x_{min,\ cell}/L$	–	8.7848×10^{-4}	–
	r_x	–	1.1092	–
	$\Delta y_{min,\ cell}/H$	–	7.0278×10^{-4}	–
	r_y	–	1.0274	–
$AR = 0.25$	$\Delta x_{min,\ cell}/L$	–	8.7848×10^{-4}	–
	r_x	–	1.1092	–
	$\Delta y_{min,\ cell}/H$	–	3.5139×10^{-3}	–
	r_y	–	1.0566	–
$AR = 0.5$	$\Delta x_{min,\ cell}/L$	1.8534×10^{-3}	8.7848×10^{-4}	4.3001×10^{-4}
	r_x	1.2303	1.1092	1.0532
	$\Delta y_{min,\ cell}/H$	3.6608×10^{-3}	1.7570×10^{-3}	8.6086×10^{-4}
	r_y	1.1741	1.0836	1.0409
$AR = 1$	$\Delta x_{min,\ cell}/L$	–	8.7848×10^{-4}	–
	r_x	–	1.1092	–
	$\Delta y_{min,\ cell}/H$	–	8.7848×10^{-4}	–
	r_y	–	1.1092	–
	Grid	M2 80 × 80	M4 80 × 160	M5 80 × 320
$AR = 2$	$\Delta x_{min,\ cell}/L$	–	8.7848×10^{-4}	–
	r_x	–	1.1092	–
	$\Delta y_{min,\ cell}/H$	–	4.3924×10^{-4}	–
	r_y	–	1.0532	–
$AR = 4$	$\Delta x_{min,\ cell}/L$	8.7848×10^{-4}	8.7848×10^{-4}	8.7848×10^{-4}
	r_x	1.1092	1.1092	1.1092
	$\Delta y_{min,\ cell}/H$	8.7848×10^{-4}	4.2750×10^{-4}	2.1962×10^{-4}
	r_y	1.1092	1.0532	1.0262
$AR = 8$	$\Delta x_{min,\ cell}/L$	–	8.7848×10^{-4}	–
	r_x	–	1.1092	–
	$\Delta y_{min,\ cell}/H$	–	5.4905×10^{-5}	–
	r_y	–	1.0371	–

Table 2
Numerical uncertainty for mean Nusselt number $\overline{Nu}$ and maximum non-dimensional vertical velocity component V_{max} on the horizontal mid-plane (i.e. $y/H = 0.5$) at $Ra_{CWHF} = 10^6$ and $Pr = 7$ for $AR = 0.5$ and 4.

	$AR = 0.5$			$AR = 4$		
	M1	M2	M3	M2	M4	M5
$\phi(\overline{Nu})$	5.3979	5.4056	5.4077	7.0783	7.0874	7.0876
ϕ_{ext}		5.408			7.088	
e_{ext} (%)	0.194	0.052	0.013	0.134	0.0056	0.0028
$\phi(V_{max})$	51.298	51.819	52.013	51.960	51.137	51.079
ϕ_{ext}		52.078			51.022	
e_{ext} (%)	1.50	0.498	0.125	1.84	0.224	0.112

3. Results and discussion

3.1. Distributions of non-dimensional temperature and velocity

The distributions of non-dimensional temperature for CWT (i.e. $\theta_{CWT} = (T - T_{cen})/(T_H - T_C)$) and CWHF (i.e. $\theta_{CWHF} = (T - T_{cen})k/qL$) configurations along the horizontal mid-plane (i.e. at $y/H = 0.5$) are shown in Fig. 2 for $Ra = 10^4 - 10^6$ and $Pr = 7.0$ where T_{cen} is the temperature at the centre of the domain. The distributions of non-dimensional vertical velocity component $V = u_2 L/\alpha$ for the corresponding cases are shown in Fig. 3. The case for which the highest mean Nusselt number $\overline{Nu} = \int_0^H h dy/k = Nu_{max}$ is obtained is also indicated in Figs. 2 and 3 by an asterisk in the legend. It can be seen from Fig. 2 that the temperature gradient $\partial T/\partial x_1$ at the vertical wall in the CWT configuration increases with increasing AR up to an aspect ratio value AR_{max} for which the maximum value of $\overline{Nu}$ is obtained. For $AR > AR_{max}$ the temperature gradient $\partial T/\partial x_1$ at the vertical wall decreases with increasing AR for the CWT configuration. In contrast, in the CWHF configuration the temperature gradient $\partial T/\partial x_1$ next to the wall must remain unchanged to satisfy the boundary condition (i.e. $-k(\partial T/\partial x_1)_{x_1=0} = q$ and $-k(\partial T/\partial x_1)_{x_1=L} = q$). It is evident from Fig. 2 that for small values of AR (e.g. $AR \ll 1.0$) the temperature profile remains linear in nature indicating conduction-dominated thermal transport. The temperature distribution becomes non-linear for high values of AR at a given value of $Ra_{CWT}(Ra_{CWHF})$ in the CWT (CWHF) configuration as the effects of convection strengthen for higher values of AR. It can be seen from Fig. 3 that the magnitude of V remains small for small values of aspect ratio indicating weak convective transport at these aspect ratios. It is evident from Fig. 3 that the magnitude of V monotonically increases with increasing AR for a given value of Ra_{CWT} in the CWT configuration. Although this trend is not strictly monotonic in the CWHF configuration, the magnitude of V attains high values for high values of AR.

It can also be observed from inspection of Figs. 2 and 3 that the temperature profile becomes increasingly non-linear and the magnitude of V increases with increasing Rayleigh number for both CWT and CWHF configurations. The strengthening of convective transport at high values of Rayleigh number can also be observed from Figs. 4 and 5 where the contours of non-dimensional temperature θ and stream function $\Psi = \psi/\alpha$ are shown respectively. The stream function is defined as $\psi = \int u_1 dx_2 - \int u_2 dx_1$ which indicates that the distributions of u_1 with x_2 and u_2 with x_1 ultimately determine the magnitude of the stream function. The distributions of streamlines in Fig. 5 are helpful in understanding the nature of the flow pattern within the enclosure. Fig. 4 shows that the isotherms remain parallel to the vertical walls at small aspect ratio indicating predominantly conduction-driven thermal transport. Moreover, the magnitude of Ψ remains small everywhere in the enclosure for small values of AR supporting the notion that convective effects are weak. Figs. 4 and 5 suggest that the effects of convection strengthen with increasing values of Ra_{CWT} and Ra_{CWHF} for a given value of AR, which is reflected in the curved isotherms and the greater magnitudes of Ψ for higher values of Rayleigh number.

3.2. Effects of Rayleigh number and aspect ratio

3.2.1. Aspect ratio effects at different Rayleigh number

Figs. 2 and 3 highlight that the value of AR_{max} decreases with increasing Ra_{CWT} in the CWT configuration. In marked contrast, in the CWHF configuration the maximum mean Nusselt number $\overline{Nu}$ is obtained for the highest value of AR irrespective of Ra_{CWHF}. It is evident from Figs. 2 and 3 that the thermal transport is predominantly confined to the boundary layer for the aspect ratio AR_{max} and thus it is important to understand the thermal transport in the boundary-layer regime for both CWT and CWHF configurations.

3.2.2. Effects of Rayleigh number on velocity magnitude

Equating the order of magnitudes of the inertial force and buoyancy force in the vertical direction yields:

$$\vartheta^2/H \sim g\beta\Delta T_{char} \tag{9}$$

where ϑ is a characteristic velocity scale and ΔT_{char} is a characteristic temperature difference which can be taken as the temperature difference between the vertical walls ΔT in the CWT configuration. For both the configurations the wall heat flux can be scaled as:

$$q \sim k\Delta T_{char}/\delta_{th} \tag{10}$$

which can be used to estimate ΔT_{char} as:

$$\Delta T_{char} \sim q\delta_{th}/k \tag{11}$$

Equating the order of magnitude of the buoyancy and viscous forces in the boundary layer gives rise to:

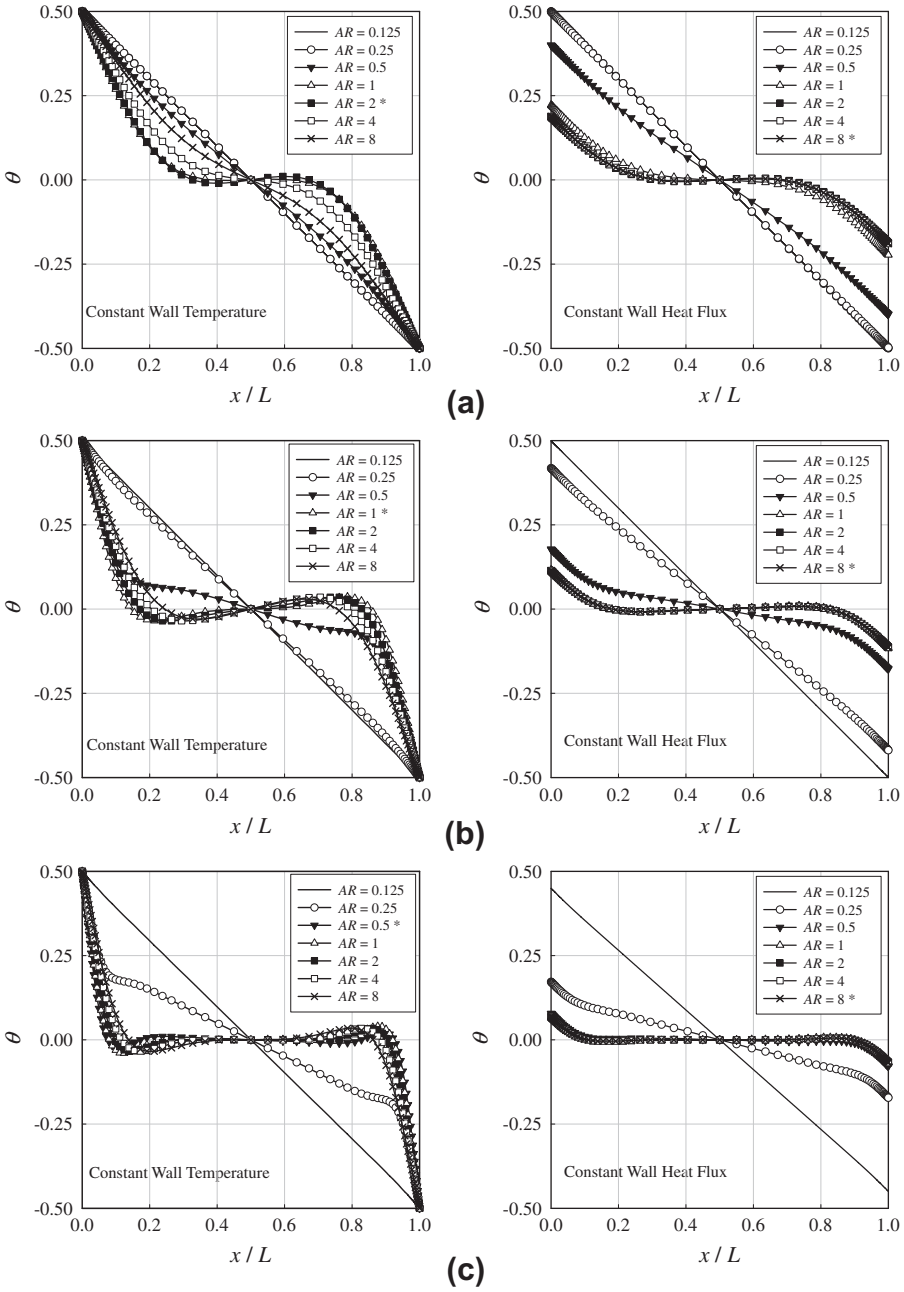

Fig. 2. Variations of non-dimensional temperature θ along the horizontal mid-plane (i.e. $y/H = 0.5$) at $Pr = 7$ for Ra_{CWHF}(Ra_{CWT}): (a) 10^4, (b) 10^5 and (c) 10^6 (* highlights the AR in which the maximum mean Nusselt number $\overline{Nu}$ occurs).

$$\rho g \beta \Delta T_{char} \sim \mu \frac{\vartheta}{\delta^2} \tag{12}$$

where δ is the hydro-dynamic boundary layer thickness.

Using Eq. (9) in Eq. (12) yields the following scaling for ϑ and δ for the CWT configuration:

$$\vartheta \sim (\alpha/L)\sqrt{Ra_{CWT} Pr AR} \text{ and } \delta \sim L(AR)^{0.25}(Pr/Ra_{CWT})^{0.25} \tag{13}$$

whereas the following scaling estimate can be obtained for the CWHF configuration:

$$\delta \sim L(AR)^{0.2}(Pr/Ra_{CWHF})^{0.2}[f_1(Ra_{CWHF}, Pr, AR)]^{0.2} \tag{14}$$

where $f_1(Ra_{CWHF}, Pr, AR)$ is a function which accounts for the ratio of hydrodynamic boundary layer thickness to thermal boundary layer thickness in the CWHF configuration. Using Eqs. (9), (11) and (14) gives rise to the following estimate of ϑ in the CWHF configuration:

$$\vartheta \sim (\alpha/L) Ra_{CWHF}^{2/5} Pr^{3/5} AR^{3/5} / f_1^{2/5} \tag{15}$$

It is worth noting that the magnitudes of the inertial, buoyancy and viscous forces remain of the same order for both CWT and CWHF boundary conditions according to the scaling estimates presented in Eqs. (13)–(15). According to Eqs. (13) and (15) the non-dimensional vertical velocity component V for the CWT and CWHF configurations scales in the following manner for the aspect ratios where the heat transfer is primarily driven by boundary layer transport:

$$V \sim \vartheta L/\alpha \sim \sqrt{Ra_{CWT} Pr AR} \text{ (for CWT) and } V \sim \vartheta L/\alpha \sim Ra_{CWHF}^{2/5} Pr^{3/5} AR^{3/5} / f_1^{2/5} \text{ (for CWHF)} \tag{16}$$

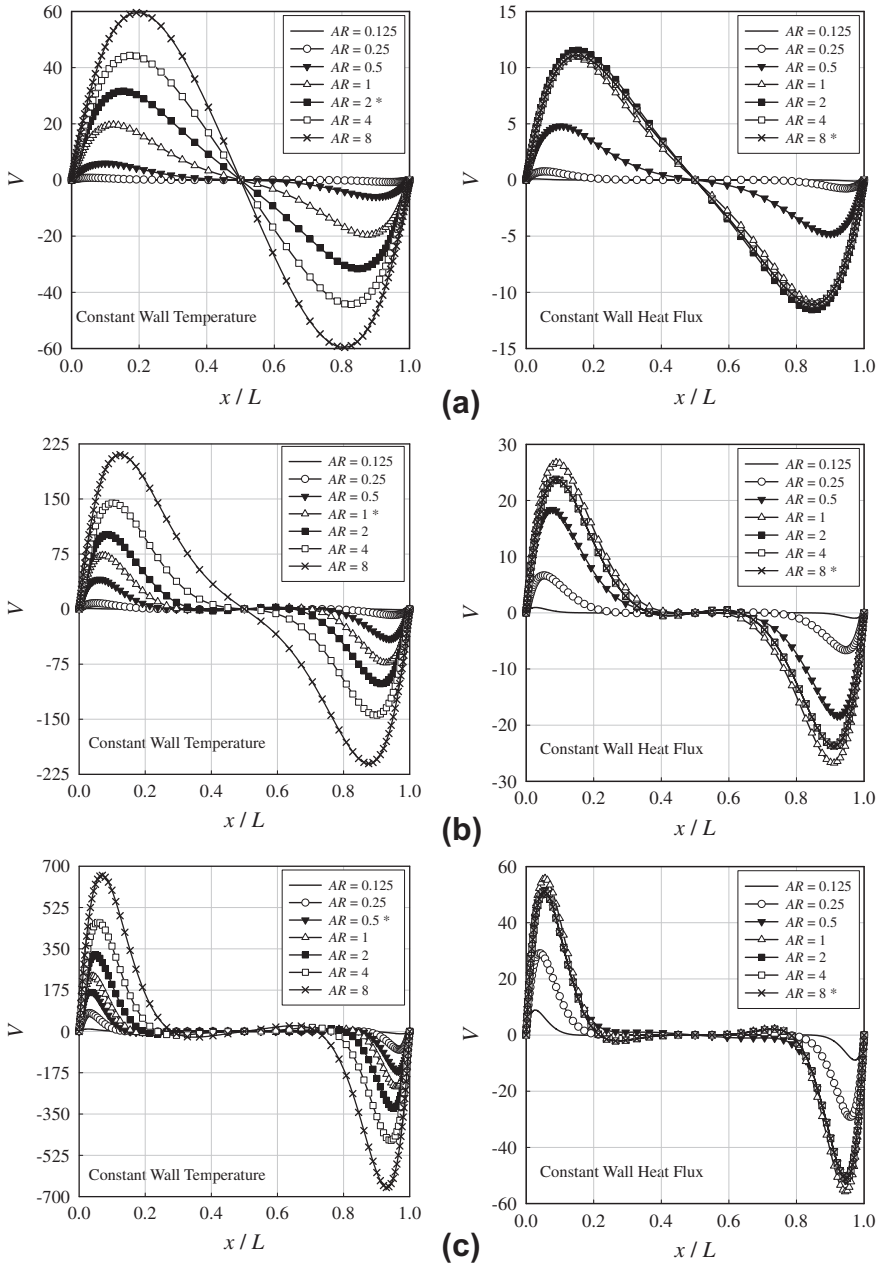

Fig. 3. Variations of non-dimensional vertical velocity component V along the horizontal mid-plane (i.e. $y/H = 0.5$) at $Pr = 7$ for Ra_{CWHF}(Ra_{CWT}): (a) 10^4, (b) 10^5 and (c) 10^6 (* highlights the AR in which the maximum mean Nusselt number $\overline{Nu}$ occurs).

Given that the above analysis is based on an order-of-magnitude estimation, the scaling relations given by Eqs. (13)–(16) (and the ones which appear later in this paper) are expected to be useful in predicting the qualitative trends but they do not necessarily yield accurate quantitative predictions. Fig. 3 shows that the magnitude of V increases with increasing AR for a given set of values of Rayleigh number, Prandtl number, α and L for both CWT and CWHF configurations where the thermal transport primarily takes place within the boundary layer (i.e. boundary layer regime according to Bejan and Tien (1978)), which is consistent with the qualitative trends predicted by Eq. (16).

3.2.3. Effects of aspect ratio and Rayleigh number on temperature difference between vertical walls

For the CWHF configuration the temperature difference between the vertical walls ΔT can be scaled as:

$$\Delta T \sim q\delta_{th}/k \sim (\Delta T)_{cond}(AR)^{0.2}(Pr/Ra_{CWHF})^{0.2}[f_1(Ra_{CWHF}, Pr, AR)]^{-0.8} \quad (17)$$

where $(\Delta T)_{cond} = qL/k$ is the temperature difference between the vertical walls under pure conduction. Eq. (17) qualitatively indicates that ΔT is expected to decrease in comparison to $(\Delta T)_{cond} = qL/k$ with increasing Ra_{CWHF} for a given value of AR, which is consistent with the observations made from Fig. 2. The temperature difference between the vertical walls for the CWHF configuration becomes exactly equal to that obtained for the CWT configuration when heat transfer takes place purely due to conduction. Thus, the temperature difference between vertical walls for the CWHF configuration remains smaller than that obtained in the CWT configuration for the same numerical values of Ra_{CWHF} and Ra_{CWT} (see Fig. 2). It is worth noting that Eq. (17) suggests that ΔT is likely to increase with AR but such a trend is not clearly visible from Fig. 2

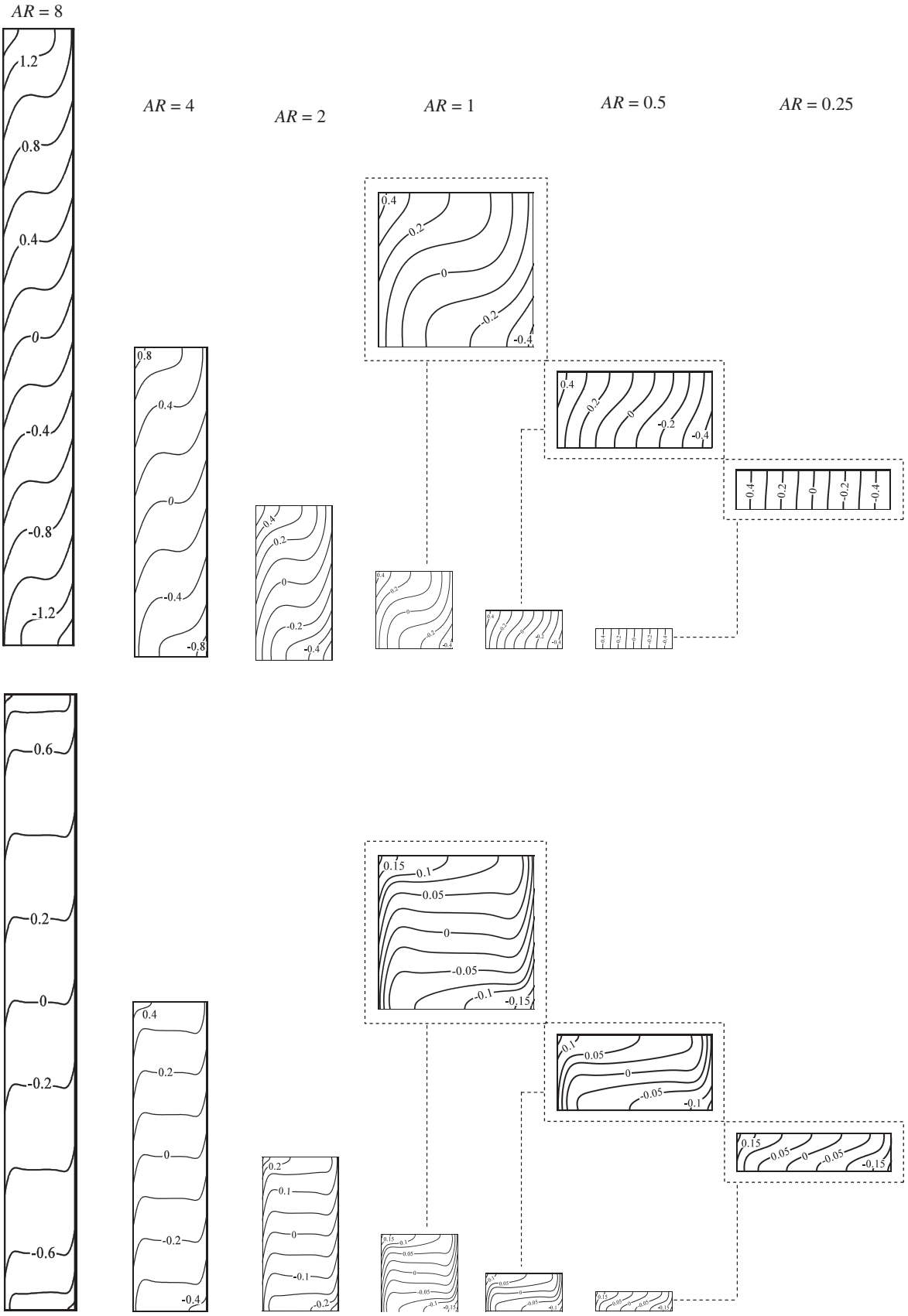

Fig. 4. Contours of non-dimensional temperature θ for convection at $Pr = 7$ for $Ra_{CWHF} = 10^4$ (1st row) and $Ra_{CWHF} = 10^6$ (2nd row).

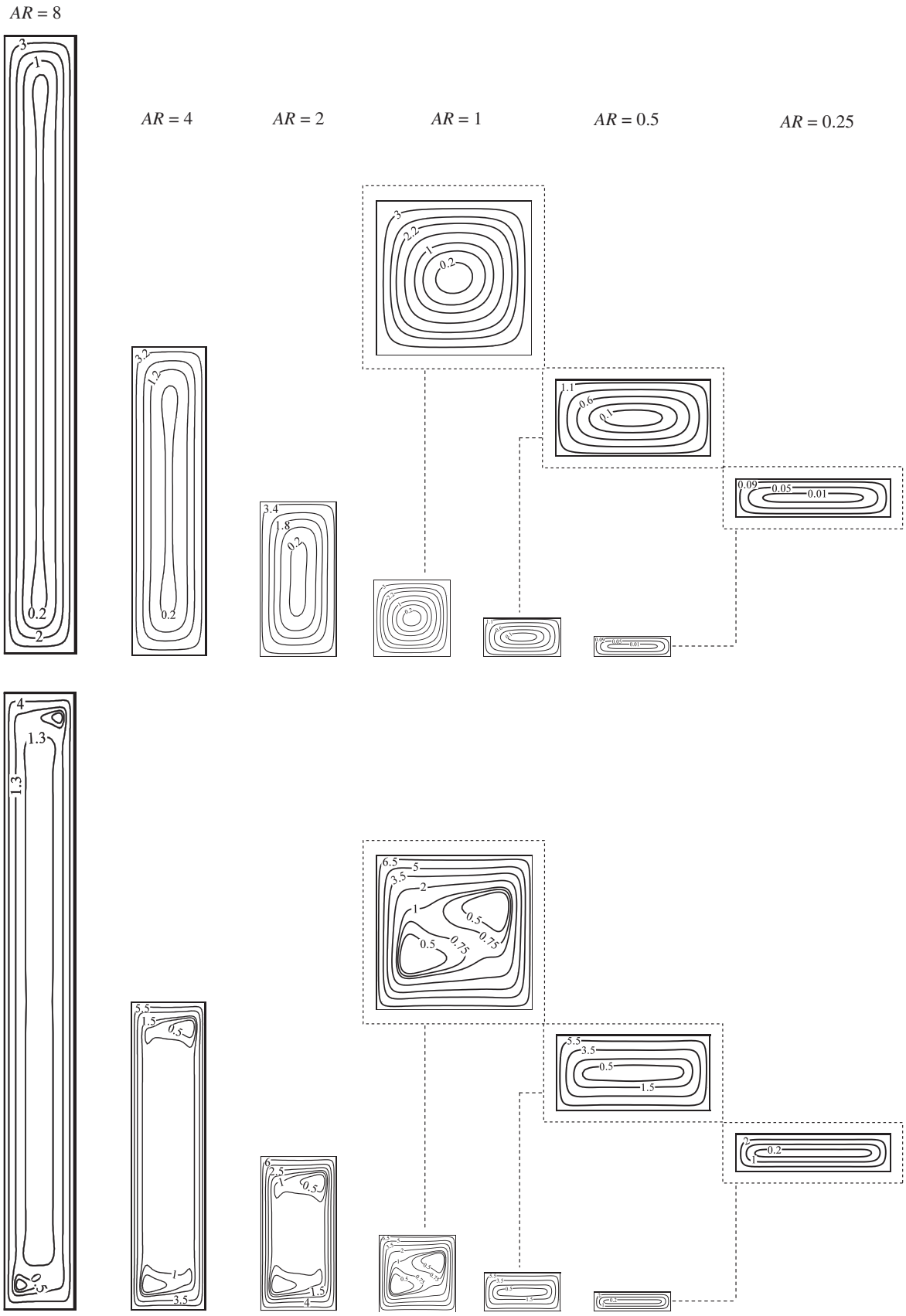

Fig. 5. Contours of non-dimensional stream functions (ψ/α) for convection at $Pr = 7$ for $Ra_{CWHF} = 10^4$ (1st row) and $Ra_{CWHF} = 10^6$ (2nd row).

for the aspect ratios where boundary-layer type transport is evident. Although both AR and Ra_{CWHF} have an exponent of 0.2 in the scaling relation given by Eq. (17), the magnitude of Ra_{CWHF} remains much greater than AR and the value of $AR^{0.2}$ remains of the order of unity for the AR values at which the boundary-layer regime is evident. Thus, the effects of Ra_{CWHF} are likely to be more prominent than the effects of AR for the parameter range explored here.

3.2.4. Effects of aspect ratio and Rayleigh number on heat flow rate

The total amount of thermal energy flow rate $\dot{Q}$ can be obtained by an energy-flux integral over any cross-section at a given height, which can be expressed in the following manner $\dot{Q} = \int_0^L [\rho c_p u_2 T - k\partial T/\partial x_2] dx_1$ for the convection regime where boundary-layer transport plays the key role (Gill, 1966; Bejan, 1979). The contribution of thermal transport due to advection within the boundary layer is given by Bejan (1979):

$$\dot{Q}_{conv} = \int_0^L \rho c_p u_2 T \, dx_1 \tag{18i}$$

As the fluid velocity outside the boundary layer becomes negligible in this configuration the integral $\int_0^L \rho c_p u_2 T dx_1$ can alternatively be written as:

$$\int_0^L \rho c_p u_2 T dx_1 \approx \int_0^\delta \rho c_p u_2 T \, dx_1 \tag{18ii}$$

The contribution of thermal diffusion to $\dot{Q}$ within the boundary layer is given by Bejan (1979):

$$\dot{Q}_{diff} = \int_0^L -k \frac{\partial T}{\partial x_2} dx_1 \tag{19}$$

Using the scaling estimate given by Eq. (13) the order of magnitude of heat transfer due to convection can be estimated as: $\dot{Q}_{conv} \sim (k\Delta T) Ra_{CWT}^{0.25} Pr^{0.75} AR^{0.75}$ for the CWT boundary condition according to Bejan et al. (1981). The maximum magnitude of $\dot{Q}_{diff}$ for the CWT boundary condition can, in turn, be estimated as: $\dot{Q}_{diff} \sim (k\Delta T) AR^{-1}$ (Bejan et al., 1981). Following similar scaling arguments as followed by Bejan et al. (1981) and using Eqs. (14), (15) and (17) the contribution of $\dot{Q}_{conv}$ can be estimated as: $\dot{Q}_{conv} = (qL) PrAR f_1^{-1}$ whereas the maximum magnitude of $\dot{Q}_{diff}$ scales as: $\dot{Q}_{diff} \sim (qL) AR^{-0.8} (Pr/Ra_{CWHF})^{0.2} f_1^{-0.8}$. The above scaling estimates indicate that the effects of convection strengthen with increasing AR whereas the thermal diffusion effects weaken with increasing AR for both the CWT and CWHF configurations. The above conclusion is in full agreement with analytical results obtained by Bejan (1979) for the CWT boundary condition. The quantities $k\Delta T$ and qL remain unchanged for the CWT and CWHF configurations and thus according to the above scaling of $\dot{Q}_{conv}$, the convective transport in the CWHF configuration strengthens more rapidly with increasing AR than in the CWT configuration for a given set of values of Rayleigh and Prandtl numbers. In contrast, according to the above scaling of $\dot{Q}_{diff}$, the thermal diffusion strength decreases more rapidly with increasing AR in the CWT configuration than in the CWHF configuration for a given set of values of Rayleigh and Prandtl numbers.

As the convection strength increases and the diffusion strength decreases significantly with increasing AR in the CWT configuration, the maximum mean Nusselt number $\overline{Nu}$ increases up to an aspect ratio AR_{max} when the strengthening of convection dominates over the weakening of thermal diffusion. However, for $AR > AR_{max}$ the mean Nusselt number $\overline{Nu}$ in the CWT configuration starts to decrease with increasing AR as the weakening of diffusion strength dominates over the strengthening of convective strength. The strengthening of convective transport relative to the weakening of diffusive thermal transport is more prevalent in the CWHF configuration than in the CWT configuration for the same numerical values of Rayleigh number, which leads to a monotonic increase in $\overline{Nu}$ with increasing AR in the CWHF configuration.

3.2.5. Effects of aspect ratio and Rayleigh number on the mean Nusselt number

The variation of $\overline{Nu}$ with AR for both the CWT and CWHF configurations at $Pr = 7$ and 0.71 are shown in Fig. 6a and b respectively. It can be seen from Figs. 6a and b that the variation of $\overline{Nu}$ with AR for $Pr = 0.71$ remains both qualitatively and quantitatively similar to the corresponding variation obtained for $Pr = 7$ in both the CWT and CWHF configurations. Thus detailed results are confined to a single Prandtl number ($Pr = 7$) in this paper for the sake of conciseness. The aforementioned non-monotonic variation of $\overline{Nu}$ with AR in the CWT configuration can be seen from Fig. 6a. The value of AR_{max} at which $\overline{Nu}$ attains its maximum value depends on the relative strengths of thermal advection and diffusion mechanisms and the scalings of $\dot{Q}_{conv}$ and $\dot{Q}_{diff}$ for the CWT boundary condition suggest that AR_{max} is expected to change with Ra_{CWT}. Fig. 6a does indeed demonstrate that the value of AR_{max} decreases with increasing Ra_{CWT}. The variation of $\overline{Nu}$ with AR for the CWT configuration is consistent with previous studies (Bejan, 1980; Dong and Zhai, 2007; Ganguli et al., 2009). As the strengthening (weakening) of thermal advection (diffusion) in the CWHF configuration with increasing AR is more (less) rapid than in the CWT configuration, the mean Nusselt number $\overline{Nu}$ increases monotonically with increasing AR in the CWHF configuration as shown in Fig. 6b.

3.2.6. Comparison between CWT and CWHF configurations

As ΔT assumes smaller values in the CWHF configuration than in the CWT configuration for the same values of Ra_{CWT} and Ra_{CWHF} (see Fig. 2 and Eq. (17)), the magnitude of the velocity induced in the CWHF case remains smaller than in the CWT case for the same numerical values of Rayleigh number (see Fig. 3). For cases where the aspect ratio is approximately one, smaller velocity magnitudes and weaker convection strength in the CWHF configuration than in the CWT configuration lead to reduced values of $\overline{Nu}$ in the CWHF case in comparison to the CWT case (for the same numerical values of Rayleigh number). However, at large values of AR (i.e. $AR > AR_{max}$) $\overline{Nu}$ begins to decrease with increasing AR for the CWT configuration whereas $\overline{Nu}$ increases monotonically with increasing AR for the CWHF configuration and this eventually gives rise to higher values of $\overline{Nu}$ in the CWHF case than the corresponding value in the CWT case for the same numerical values of Rayleigh number (see Fig. 6a and b).

It can be concluded from Eqs. (18i) and (19) that the advective thermal transport starts to overcome the thermal diffusive transport when $(k\Delta T) Ra_{CWT}^{0.25} Pr^{0.75} AR^{0.75} > (k\Delta T) AR^{-1}$ which suggests that for $Ra_{CWT} > Pr^{-3} AR^{-7}$ convection plays a key role in thermal transport. This is consistent with the criterion (i.e. $Ra_{CWT} > AR^{-7}$) proposed by Bejan et al. (1981). Similarly for the CWHF configuration advection starts to overcome the diffusive transport when $(qL) PrAR f_1^{-1} > (qL) AR^{-0.8} (Pr/Ra_{CWHF})^{0.2} f_1^{-0.8}$ which implies for $Ra_{CWHF} > Pr^{-4} AR^{-9}$ convection plays a key role in the CWHF configuration. This suggests that convection plays a significant role and the boundary-layer regime of convection can be realised for all the $AR \geqslant 1$ cases in both CWT and CWHF configurations. According to the above criteria the values of $Ra_{CWT}(Ra_{CWHF})$ above which convective transport is important for $AR = 0.125$, 0.25 and 0.5 are of the order of 10^6, 10^4 and 10^2 (10^8, 10^5 and 10^2) for the CWT (CWHF) configuration respectively.

3.3. Behaviour of mean Nusselt number $\overline{Nu}$ and Nusselt number correlations

3.3.1. Nusselt number scaling for the boundary-layer regime

The heat transfer coefficient h can be scaled as:

$$q \sim k\Delta T/\delta_{th} \sim h\Delta T \tag{20i}$$

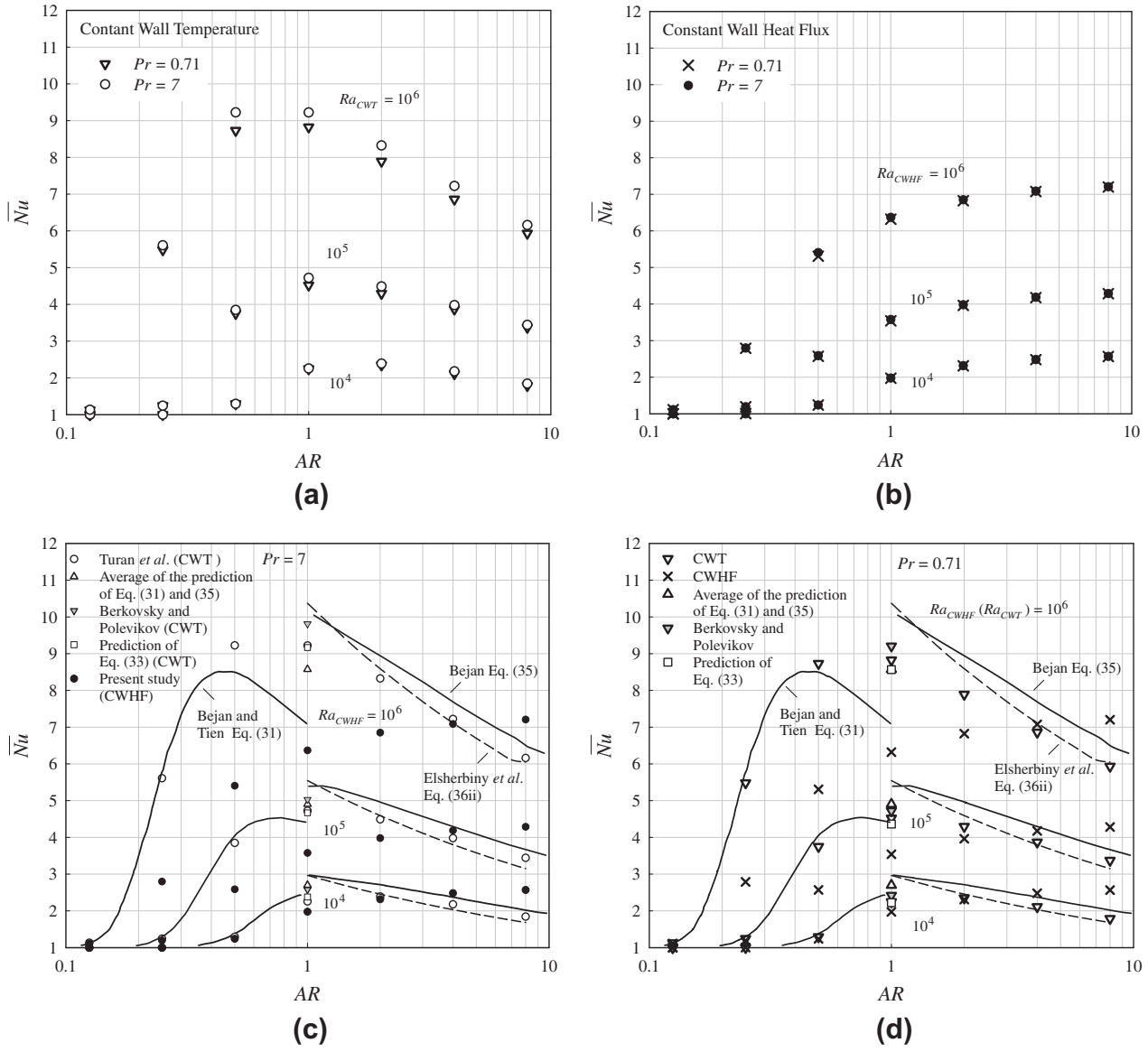

Fig. 6. Comparison between the variations of mean Nusselt number $\overline{Nu}$ with aspect ratio AR for $Pr = 0.71$ and 7.0 at Ra_{CWHF} (Ra_{CWT}) = 10^4, 10^5 and 10^6 for (a) constant wall temperature (CWT) and (b) constant wall heat flux (CWHF) boundary conditions. Variations of mean Nusselt number $\overline{Nu}$ with aspect ratio AR at Ra_{CWHF}(Ra_{CWT}) = 10^4,10^5 and 10^6 for constant wall temperature (CWT) and constant wall heat flux (CWHF) boundary conditions along with the predictions of existing correlations for (c) $Pr = 7$, (d) $Pr = 0.71$.

Based on Eq. (20i) the mean Nusselt number $\overline{Nu}$ can be estimated as:

$$\overline{Nu} = \frac{hL}{k} \sim \frac{L}{\delta_{th}} \tag{20ii}$$

Using the scaling for δ from Eqs. (13) and (14) one obtains:

$$\overline{Nu} \sim \left(\frac{Ra_{CWT}}{PrAR}\right)^{1/4} f_2(Ra_{CWT}, Pr, AR) \text{ (for CWT)};$$
$$\overline{Nu} \sim \left(\frac{Ra_{CWHF}}{PrAR}\right)^{1/5} [f_1(Ra_{CWHF}, Pr, AR)]^{0.8} \text{(for CWHF)} \tag{20iii}$$

where $f_2(Ra_{CWT}, Pr, AR)$ is a function which accounts for the ratio of hydrodynamic boundary layer thickness to thermal boundary layer thickness in the CWT configuration. A similar scaling of $\overline{Nu}$ for the CWT configuration was also reported by Bejan (1979).

3.3.2. Scaling of velocity magnitude for the parallel-flow regime

In the parallel-flow regime the vertical velocity component at the core of the enclosure vanishes and the fluid flow in the enclosure is made up of two counter-flowing horizontal streams and the temperature gradient in the horizontal direction $K = \partial T/\partial x_1 \sim \Delta T/L \sim q/k$ remains constant. Under this condition the steady-state vorticity (i.e. $\omega = (\partial u_2/\partial x_1 - \partial u_1/\partial x_2)$) transport equation takes the following form:

$$\rho u_j \frac{\partial \omega}{\partial x_j} = \rho g \beta \frac{\partial T}{\partial x_1} + \frac{\partial^2 \tau_{21}}{\partial x_1 \partial x_1} + \frac{\partial^2 \tau_{22}}{\partial x_1 \partial x_2} - \frac{\partial^2 \tau_{11}}{\partial x_1 \partial x_2} - \frac{\partial^2 \tau_{12}}{\partial x_2 \partial x_2} \tag{21i}$$

The term on the left hand side of Eq. (21i) accounts for advection of vorticity whereas the first term on right hand side indicates the vorticity generation/destruction due to buoyancy and the last four terms on the right hand side of Eq. (21i) indicate the molecular diffusion of vorticity. The contribution of $(-\partial^2 \tau_{12}/\partial x_2^2)$ is the leading-order contributor to the vorticity diffusion and the asymptotic analysis by Cormack et al. (1974a) indicates an equilibrium is maintained between the buoyancy and viscous contributions at the core region of the enclosure for the parallel-flow regime (Bejan and Tien, 1978). Equating the order of magnitude of vorticity generation/destruction by buoyancy and the molecular diffusion of vorticity at the middle of the domain yields:

$$\rho g\beta K \sim -\frac{\partial^2 \tau_{12}}{\partial x_2^2} \text{ or } \rho g\beta \frac{\Delta T}{L} \sim \frac{\partial}{\partial x_2^2}\left[\mu \frac{\partial u_1}{\partial x_2}\right] \text{ or } \rho g\beta \frac{\Delta T}{L} \sim \frac{\mu u_c}{F^3 H^3} \quad (21ii)$$

which leads to the following scaling for the horizontal velocity component at the core:

$$u_c \sim F^3(\rho g\beta K H^3/\mu) \quad (21iii)$$

where the hydrodynamic boundary layer thickness on the horizontal surfaces is scaled as: $\delta \sim FH$ with F being an appropriate fraction (i.e. $0 < F < 1$). Thus u_c scales in the following manner for the CWT and CWHF configurations:

$$u_c \sim (\alpha/L)F_{CWT}^3 Ra_{CWT} AR^3 \text{ (for CWT)}; u_c \sim (\alpha/L)F_{CWHF}^3 Ra_{CWHF} AR^3 \text{ (for CWHF)} \quad (21iv)$$

It is worth noting that the asymptotic analysis by Cormack et al. (1974a) also suggests $u_c \sim (\alpha/L)Ra_{CWT}AR^3$ for the CWT configuration whereas Eq. (21iv) is derived here based on scaling arguments.

Equating the order of magnitudes of the convective and diffusive terms of the energy transport equation gives the following relation for the CWT configuration:

$$\rho c_p u_1 \frac{\partial T}{\partial x_1} \sim k\frac{\partial^2 T}{\partial x_2^2} \text{ or } \rho c_p u_c \frac{\Delta T}{L} \sim k\frac{\Delta T_1}{F_{CWT}^2 H^2} f_3(Ra_{CWT}, Pr)^2 \quad (21v)$$

where ΔT_1 is the characteristic temperature difference between the horizontal adiabatic walls and the thermal boundary layer thickness adjacent to the horizontal walls is scaled as: $\delta_{th} \sim FH/f_3(Ra_{CWT}, Pr)$. Eq. (21iv) yields the following relation for the CWT configuration:

$$\rho c_p u_c K \sim \frac{k}{L^2}\Delta T F_{CWT}^3 Ra_{CWT} AR^3 \sim \frac{k f_3^2}{F_{CWT}^2 H^2}\Delta T_1 \text{ or } \Delta T_1 \sim Ra_{CWT} F_{CWT}^5 AR^5 \Delta T / f_3(Ra_{CWT}, Pr)^2 \quad (21vi)$$

Eq. (21iv) is derived here based on scaling arguments but it is in excellent agreement with analytical results by Cormack et al. (1974a) who also indicated that ΔT_1 scales as $\Delta T_1 \sim Ra_{CWT}AR^5\Delta T$ in the CWT configuration.

Equating the order of magnitudes of the advective and diffusive terms of the energy transport equation for the CWHF configuration yields:

$$\rho c_p u_1 \frac{\partial T}{\partial x_1} \sim k\frac{\partial^2 T}{\partial x_2^2} \text{ or } \rho c_p u_c \frac{q}{k} \sim k\frac{\Delta T_1}{F_{CWHF}^2 H^2} f_4(Ra_{CWHF}, Pr)^2 \quad (21vii)$$

Using Eq. (21iv) in Eq. (21vii) gives:

$$\Delta T_1 \sim Ra_{CWHF} F_{CWHF}^5 AR^5 \frac{qL}{k}\frac{1}{f_4^2} \quad (21viii)$$

where the temperature difference between the vertical walls ΔT in the CWHF configuration remains of the order of qL/k in the parallel-flow regime (i.e. $\Delta T \sim qL/k$).

3.3.3. Scaling of mean Nusselt number in the parallel flow regime

3.3.3.1. CWT configuration. The mean Nusselt number $\overline{Nu}$ can be estimated by carrying out an energy flux analysis over any vertical cross-section (Bejan and Tien, 1978):

$$\overline{Nu} = \frac{L}{Hk\Delta T}\int_0^H \left[\rho c_p u_1 T - k\frac{\partial T}{\partial x_1}\right] dx_2 = \overline{Nu}_1 + \overline{Nu}_2 \quad (22i)$$

where $\overline{Nu}_1$ and $\overline{Nu}_2$ originate due to convective and diffusive effects which are given by:

$$\overline{Nu}_1 = \frac{L}{Hk\Delta T}\int_0^H \rho c_p u_1 T dx_2 \text{ and } \overline{Nu}_2 = -\frac{L}{Hk\Delta T}\int_0^H k\frac{\partial T}{\partial x_1} dx_2 \quad (22ii)$$

Using Eqs. (21iv) and (21vi) $\overline{Nu}_1$ can be scaled for the CWT configuration as:

$$\overline{Nu}_1 = \frac{L}{Hk\Delta T}\int_0^H \rho c_p u_1 T dx_2 \sim \frac{L\rho c_p u_c \Delta T_1 H}{Hk\Delta T} \sim Ra_{CWT}^2 F^8 AR^8 / f_3^2 \quad (22iii)$$

whereas $\overline{Nu}_2$ can be scaled as:

$$\overline{Nu}_2 = -\frac{L}{Hk\Delta T}\int_0^H k\frac{\partial T}{\partial x_1} dx_2 = \frac{H\Delta T L k}{H\Delta T L k} = 1 \quad (22iv)$$

Thus in the parallel-flow regime (i.e. $Ra_{CWT}AR^3 \to 0$) the mean Nusselt number $\overline{Nu}$ can be given in the following way for the CWT configuration:

$$\overline{Nu} = 1 + a_{CWT} Ra_{CWT}^2 F_{CWT}^8 AR^8 / f_3^2 \quad (22v)$$

where a_{CWT} is an appropriate constant. It is worth noting that Eq. (22v), which is derived here based on scaling arguments, is in remarkable agreement with the expression $Nu_A = 1 + Ra_{CWHF}^2 AR^8/362880$ obtained by Cormack et al. (1974a) based on asymptotic analysis.

3.3.3.2. CWHF configuration. Using Eqs. (21iv) and (21viii) the Nusselt number $\overline{Nu}_1$ in the CWHF configuration can be estimated as:

$$\overline{Nu}_1 = \frac{L}{Hk\Delta T}\int_0^H \rho c_p u_1 T dx_2 \sim \frac{L\rho c_p u_c \Delta T_1 H}{Hk(qL/k)} \sim Ra_{CWHF}^2 F_{CWHf}^8 AR^8 / f_4^2 \quad (23i)$$

whereas $\overline{Nu}_2$ can be scaled as:

$$\overline{Nu}_2 = -\frac{L}{Hk\Delta T}\int_0^H k\frac{\partial T}{\partial x_1} dx_2 = \frac{LqH}{Hk(qL/k)} = 1 \quad (23ii)$$

Thus in the parallel-flow regime (i.e. $Ra_{CWHF}AR^3 \to 0$) the mean Nusselt number $\overline{Nu}$ can be given in the following manner for the CWHF configuration:

$$\overline{Nu} = 1 + a_{CWHF} Ra_{CWHF}^2 F_{CWHF}^8 AR^8 / f_4^2 \quad (23iii)$$

where a_{CWHF} is an appropriate constant.

3.3.4. Nusselt number correlations for CWT configuration

The variations of $\overline{Nu}$ shown in Fig. 6a and b are now replotted in Fig. 6c and d for $Pr = 7$ and 0.71 respectively to show $\overline{Nu}$ values for both the CWT and CWHF boundary conditions and for the purpose of comparing the performance of the existing correlations for the CWT boundary condition. Eqs. (22v) and (23iii) indicate that $\overline{Nu}$ for small values of AR (i.e. $AR \ll 1$) attains comparable values for the same numerical values of Ra_{CWT} and Ra_{CWHF} in both the CWT and CWHF configurations. This feature can be confirmed from Fig. 6c and d which show that $\overline{Nu}$ at identical values of Ra_{CWT} and Ra_{CWHF} remain almost the same for small values of AR in both the CWT and CWHF configurations (see $AR = 0.125$ case in Fig. 6c and d). However in the CWT configuration the convective transport starts to play a key role at a much smaller value of Rayleigh number than that in the CWHF configuration and, as a result of this, the mean Nusselt number $\overline{Nu}$ in the CWHF configuration is smaller than in the CWT configuration for the $AR = 0.25$ and 0.5 cases at the same numerical values of Ra_{CWT} and Ra_{CWHF} (see Fig. 6c and d).

3.3.4.1. Correlations for the parallel-flow regime. Cormack et al. (1974a) carried out an asymptotic analysis in the CWT configuration for the $Ra_{CWT}AR^3 \to 0$ limit and obtained the following expression for the mean Nusselt number (i.e.$\overline{Nu} = \int_0^H Nudx_2/H$):

$$\overline{Nu} = 1 + Ra_{CWT}^2 AR^8/362880 \tag{24}$$

It is worth noting that the analytical result given by Eq. (24) is remarkably similar to the scaling estimate given by Eq. (22v). The temperature difference between the horizontal walls ΔT_1 in the $Ra_{CWT}AR^3 \to 0$ limit is given by (Cormack et al., 1974a):

$$\Delta T_1 = Ra_{CWT}AR^5\Delta T/720 \tag{25}$$

Bejan and Tien (1978) argued that $\Delta T_1 \leqslant \Delta T/10$ in the parallel-flow regime (i.e.$Ra_{CWT}AR^3 \to 0$) which yields the following criterion for this regime:

$$Ra_{CWT} < 72(AR)^{-5} \tag{26}$$

The other extreme convection condition is referred to as the 'boundary-layer regime' by Bejan and Tien (1978) where Ra_{CWT} assumes large values and ΔT_1 remains comparable to ΔT (i.e. $\Delta T_1 \sim \Delta T$).

3.3.4.2. Correlations for the boundary-layer regime. In the boundary-layer regime the high values of temperature gradient are confined to two thin boundary layers adjacent to the vertical walls. Bejan and Tien (1978) obtained the following correlation for the boundary-layer regime for the CWT configuration:

$$\overline{Nu} = 0.623Ra_{CWT}^{1/5}AR^{-2/5} \tag{27}$$

In this regime the horizontal temperature gradient is given by:

$$K = \frac{\partial T}{\partial x_1} \sim 60.93Ra_{CWT}^{3/5}AR^{9/5}\frac{\Delta T}{H} \tag{28}$$

Bejan and Tien (1978) argued that the inception of the boundary-layer regime can be indicated by $K < 0.1(\Delta T/L)$ which gives rise to the following criterion:

$$Ra_{CWT} > 4.4 \times 10^4 AR^{-14/3} \tag{29}$$

Some of the characteristics of both the boundary layer and $Ra_{CWT}\,AR^3 \to 0$ regimes are observed if the Rayleigh number Ra_{CWT} falls in the range:

$$72(AR)^{-5} < Ra_{CWT} < 4.4 \times 10^4 AR^{-14/3} \tag{30}$$

Bejan and Tien (1978) termed this as the 'intermediate regime'. Bejan and Tien (1978) combined Eqs. (24) and (27) to come up with the following correlation which can be applied for all the three aforementioned regimes:

$$\overline{Nu} = 1 + \left[\left(Ra_{CWT}^2 AR^8/362880\right)^n + \left(0.623Ra_{CWT}^{1/5}AR^{-2/5}\right)^n\right]^{1/n} \text{ where } n = -0.386 \tag{31}$$

Berkovsky and Polevikov (1977) proposed the following correlation for square enclosures including Prandtl number effects in the CWT configuration:

$$\overline{Nu} = 0.18\left(\frac{Ra_{CWT}Pr}{0.2+Pr}\right)^{0.29} \tag{32}$$

Recently the present authors (Turan et al., 2010) proposed a new correlation for square enclosures which was shown to provide better agreement with the predictions of numerical simulations for the CWT configuration (Shyy and Chen, 1990; Turan et al., 2010) than the correlation proposed by Berkovsky and Polevikov (1977):

$$\overline{Nu} = 0.162Ra_{CWT}^{0.293}\left(\frac{Pr}{1+Pr}\right)^{0.091} \tag{33}$$

Eq. (33) is qualitatively consistent with the scaling estimation given by Eq. (20iii), which suggested $\overline{Nu} \sim (Ra_{CWT}/Pr)^{1/4} f_2(Ra_{CWT}, Pr)$ and, given the simplicity of the scaling analysis, the small difference in the exponent of Rayleigh number is not surprising.

For tall enclosures (i.e. $AR \gg 1$ but in practice usually $20 > AR > 2$) the mean Nusselt number for the CWT configuration is often expressed as: $\overline{Nu} = c_1 Ra_{CWT}^{c_2} AR^{c_3}$ and Bejan's analysis (Bejan, 1979) demonstrated that the constants c_1, c_2 and c_3 are functions of Ra_{CWT} and AR. Bejan (1979) also showed that the analytical results of Gill (1966) leads to the following expression of $\overline{Nu}$ for extremely large values of aspect ratio (i.e. $Ra_{CWT}^{1/7}AR \to \infty$):

$$\overline{Nu} = 0.364[Ra_{CWT}/(PrAR)]^{1/4} \tag{34}$$

According to Bejan (1979) $\overline{Nu}$ for tall enclosures is given by:

$$\overline{Nu} = C_B[Ra_{CWT}/(PrAR)]^{1/4}\int_{-q_e}^{q_e}\frac{(1-q_f)^6(1+q_f)^2(7-q_f^2)}{(1+q_f^2)(1+3q_f^2)^{14/3}}dq_f \tag{35}$$

where C_B and q_e are functions of $Ra^{1/7}AR$ and C_B (q_e) is found to decrease (increase) from 1.0 to 0.912 (0.1 to 1.0) with increase in $Ra_{CWT}^{1/7}AR$ from 0 to 1000 (Bejan, 1979). Bejan (1979) found that $\overline{Nu}$ for tall enclosures deviate from the asymptotic value when $Ra_{CWT}^{1/7}AR < 100$ and the prediction of Eq. (35) approaches to that of Eq. (34) for $(Ra_{CWT}/AR)^{1/4} \geqslant 10$.

Different mean Nusselt number correlations for the CWT configuration have been proposed for tall enclosures based on experimental (Yin et al., 1978; Elsherbiny et al., 1982; Wakitani, 1996) and computational (Lee and Korpela, 1983; Le Quéré, 1990; Wakitani, 1997; Zhao et al., 1997; Frederick, 1999; Lartigue et al., 2000; Dong and Zhai, 2007; Ganguli et al. (2009)) studies and interested readers are referred to Ganguli et al. (2009) for an extensive review and the assumptions behind the respective correlations. One of the most used correlations for tall enclosures with $AR > 5$ for the CWT boundary condition was proposed by Elsherbiny et al. (1982):

$$\overline{Nu} = Max(Nu_{1c}, Nu_{2c}, N_{3c}) \tag{36i}$$

where Nu_{1c}, Nu_{2c} and Nu_{3c} are given by:

$$Nu_{1c} = 0.0605Ra_{CWT}^{1/3};$$

$$Nu_{2c} = \left[1 + \left[\frac{0.104Ra_{CWT}^{0.293}}{1+(6310/Ra_{CWT})^{1.36}}\right]^3\right]^{1/3} \text{ and}$$

$$Nu_{3c} = 0.242(Ra_{CWT}/AR)^{0.272} \tag{36ii}$$

The performance of the aforementioned correlations for the mean Nusselt number will be compared to $\overline{Nu}$ obtained from numerical simulations in the next sub-section.

3.3.5. Predictions of correlations for CWT configuration

Fig. 6c and d demonstrate that Eq. (31) proposed by Bejan and Tien (1978) satisfactorily captures the variation of $\overline{Nu}$ with AR for $AR < 1$ and the agreement between the prediction of Eq. (31) and the numerical results improves with decreasing aspect ratio. However, this expression underpredicts the value of $\overline{Nu}$ for the aspect ratios of the order of unity (i.e. $AR \sim 1$). The extent of this underprediction increases with increasing value of Ra_{CWT}. Eq. (35) proposed by Bejan (1979) satisfactorily predicts the mean Nusselt number $\overline{Nu}$ with AR for large values of aspect ratio (i.e. $AR \gg 1$). However, the expression by Bejan (1979) overpredicts $\overline{Nu}$ for aspect ratio equal to unity and the extent of this overprediction increases with increasing Ra_{CWT}. The correlation (Eq. (36ii)) by Elsherbiny et al. (1982), although only proposed for $AR > 5$, exhibits satisfactory quantitative agreement with the present simulation data for tall enclosures with $AR \geqslant 2$ (see Fig. 6c and d). However, the correlation by Elsherbiny et al. (1982) (Eq. (36ii)) also

overpredicts the value of $\overline{Nu}$ for square enclosures for all the values of Rayleigh number considered in this study (see Fig. 6c and d). The arithmetic mean of the predictions of Eqs. (31) and (35) yield a satisfactory agreement with numerical prediction of $\overline{Nu}$ for $AR = 1.0$ as demonstrated in Fig. 6c and d. The predictions of the correlations proposed by Berkovsky and Polevikov (1977) (Eq. (32)) and Turan et al. (2010) (Eq. (33)) for square enclosures are also shown in Fig. 6c and d, which indicates that both Eqs. (32) and (33) satisfactorily predict $\overline{Nu}$ for square enclosures.

3.3.6. Correlations for CWHF configuration and their assessment

3.3.6.1. Correlation for AR > 1. Eq. (20iii) suggests that the mean Nusselt number $\overline{Nu}$ for a square enclosure is expected to scale as $\overline{Nu} \sim (Ra_{CWHF}/Pr)^{1/5}[f_1(Ra_{CWHF}, Pr)]^{0.8}$ and based on this scaling analysis a correlation for square enclosure in the CWHF configuration is suggested here in the following form:

$$\overline{Nu} = 0.209 Ra_{CWHF}^{0.249}\left(\frac{Pr}{1+Pr}\right)^{0.031} \tag{37i}$$

which is sufficiently close to the Rayleigh number dependence predicted by the scaling estimate in Eq. (20iii) to give confidence in this approach. For $8 \geqslant AR > 1$ cases a correlation is proposed for $\overline{Nu}$ in the following manner by analyzing the simulation results:

$$\overline{Nu} = 0.209 Ra_{CWHF}^{0.249}\left(\frac{Pr}{1+Pr}\right)^{0.031}(c_A \ln AR + 1) \tag{37ii}$$

where c_A is a correlation parameter. It is worth noting that the expression given by Eq. (37ii) compares well with the qualitative trend predicted by the scaling estimate given by Eq. (20iii) although the exponent of Ra_{CWHF} in Eq. (37ii) is slightly different from Eq. (20iii) and the function $(c_A \ln AR + 1)$ is empirically proposed to capture the mean Nusselt number $\overline{Nu}$ variation with AR. Fig. 7a and b show that Eq. (37ii) satisfactorily predicts $\overline{Nu}$ obtained from simulation data in the Rayleigh number range $10^4 \leqslant Ra_{CWHF} \leqslant 10^6$ when c_A is taken to be $c_A = 0.737 Ra_{CWHF}^{-0.189}$.

3.3.6.2. Correlation for AR < 1. For the parallel-flow regime, conduction remains the principal mode of heat transfer and the temperature distribution within the enclosure for both the CWT and CWHF boundary condition becomes identical in nature. Thus it can be expected that Eq. (24) is likely to work also in the CWHF configuration when Ra_{CWT} is replaced by Ra_{CWHF} in this limiting condition. Based on this limiting condition the mean Nusselt number $\overline{Nu}$ for the aspect ratio range $1/8 \leqslant AR \leqslant 1$ is proposed here in the following manner for the Rayleigh number range $10^4 \leqslant Ra_{CWHF} \leqslant 10^6$:

$$\overline{Nu} = Nu_A \text{ when } Ra_{CWHF}AR^3 < 10^3 \text{ and}$$
$$\overline{Nu} = Nu_B \text{ when } Ra_{CWHF}AR^3 \geqslant 10^3 \tag{38i}$$

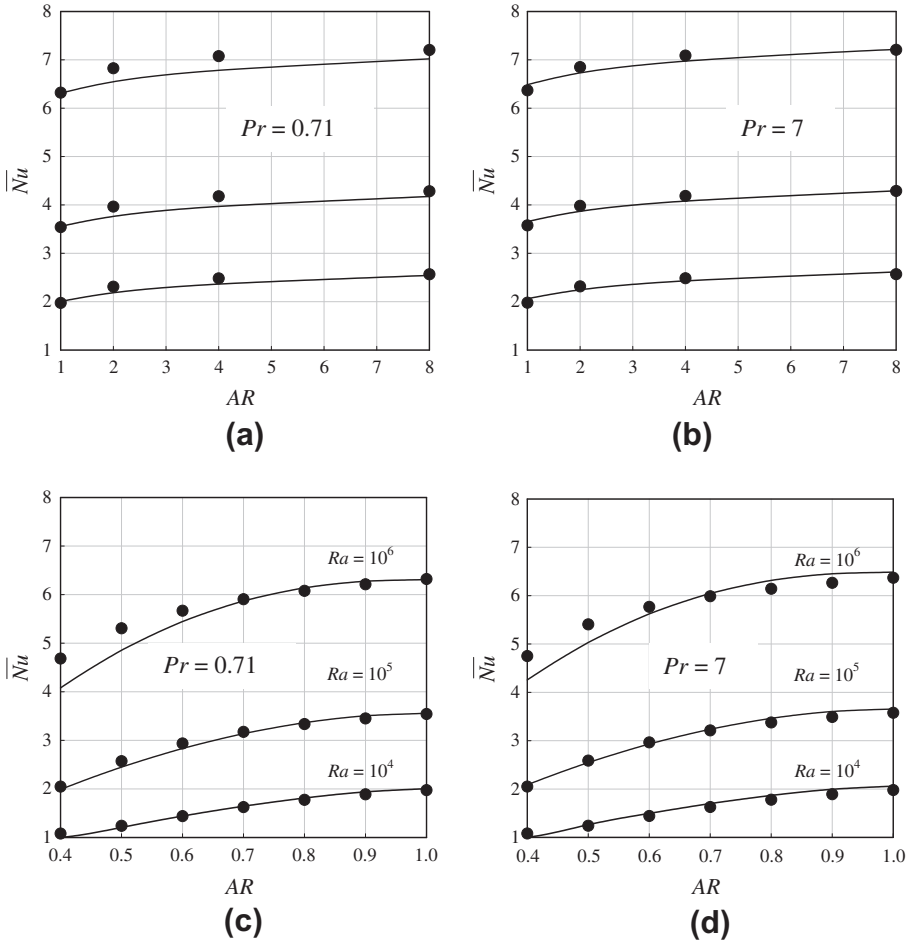

Fig. 7. Variation of mean Nusselt number $\overline{Nu}$ with aspect ratio AR (•) for the CWHF boundary condition along with the prediction of the correlation for $AR > 1$ (Eq. (37ii)) (–) at: (a) $Pr = 0.71$, (b) $Pr = 7$. Variation of mean Nusselt number $\overline{Nu}$ with aspect ratio AR (•) for the CWHF boundary condition along with the prediction of the correlation for $AR < 1$ (Eq. (38iii)) (–) at: (c) $Pr = 0.71$, (d) $Pr = 7$.

where

$Nu_A = 1 + Ra^2_{CWHF} AR^8/362880$ and

$$Nu_B = 0.209 Ra^{0.249}_{CWHF}\left(\frac{Pr}{1+Pr}\right)^{0.031}(c_B(1-AR)^{c_C}+1) \quad (38ii)$$

where c_B and c_C are given by:

$$c_B = -1.168 \text{ and } c_C = 0.683 Ra^{0.089}_{CWHF} \quad (38iii)$$

Fig. 7c and d shows that the correlation given by Eq. (38iii) satisfactorily predicts the variation of $\overline{Nu}$ for all the $AR \leqslant 1$ cases considered here.

4. Conclusions

The effects of constant wall temperature and constant wall heat flux boundary conditions at the vertical side walls on laminar steady-state natural convection of Newtonian fluids in rectangular enclosures with aspect ratios (height:width) ranging from 1/8 to 8 have been numerically studied. The simulations cover a wide range of Rayleigh number ranging from 10^4 to 10^6 for two Prandtl numbers $Pr = 0.71$ and 7.0. The mean Nusselt number $\overline{Nu}$ is found to increase with increasing values of Rayleigh number for both the CWT and CWHF boundary conditions. It has been shown that for the CWT boundary condition the mean Nusselt number $\overline{Nu}$ increases with increasing aspect ratio AR up to an aspect ratio AR_{max} where $\overline{Nu}$ attains its maximum value and for $AR > AR_{max}$ the mean Nusselt number $\overline{Nu}$ decreases with increasing AR, which is entirely consistent with several previous studies. In contrast, the mean Nusselt number $\overline{Nu}$ increases monotonically with increasing AR in the case of CWHF boundary condition for all of the aspect ratios considered here. However, at large values of AR the mean Nusselt number $\overline{Nu}$ reaches an asymptotic value for the CWHF boundary condition. Using scaling arguments it is shown that the convective thermal transport strengthens whereas the diffusive transport weakens with increasing AR for both boundary conditions. However, the strengthening of convective transport relative to the weakening of diffusive thermal transport is more prevalent in the CWHF condition than in the CWT configuration for the same numerical values of Rayleigh number, which leads to a monotonic increase in $\overline{Nu}$ with increasing AR in the CWHF configuration. It has been demonstrated that $\overline{Nu}$ values obtained from the two boundary conditions are sufficiently different that the correlations developed for the CWT boundary condition cannot be used to accurately predict $\overline{Nu}$ in the CWHF configuration for the same numerical values of Rayleigh number. The appropriate correlations for the CWT configuration have been identified based on the comparison with simulation data and new correlations have been developed for the CWHF boundary condition which are shown to capture the mean Nusselt number $\overline{Nu}$ variation with AR for aspect ratio and Rayleigh number ranges given by $1/8 \leqslant AR \leqslant 8$ and $10^4 \leqslant Ra_{CWHF} \leqslant 10^6$.

Appendix A. Non-dimensional governing equations and boundary conditions

It is possible to non-dimensionalise the spatial co-ordinates, velocity components, pressure and temperature in the following manner:

$$x_i^+ = x_i/L, \quad u_i^+ = u_i/U_{ref}, \quad P^+ = P/\rho U^2_{ref} \quad \text{and}$$
$$\theta = (T - T_{ref})/\Delta T_{ref} \quad (A1)$$

where U_{ref} is the reference velocity scale and ΔT_{ref} is a reference temperature difference. For the CWT configuration ΔT_{ref} can be taken to be $\Delta T = (T_H - T_C)$ whereas ΔT_{ref} can be taken to be equal to qL/k (i.e. $\Delta\ T_{ref} = qL/k$) for the CWHF configuration. Using $U_{ref} = \alpha/L$ in Eqs. (6)–(8) yield the following forms of non-dimensional mass, momentum and energy conservation equations:

A.1. Non-dimensional mass conservation equation

$$\frac{\partial u_i^+}{\partial x_i^+} = 0 \quad (A2)$$

A.2. Non-dimensional momentum conservation equations

$$u_j^+ \frac{\partial u_i^+}{\partial x_j^+} = -\frac{\partial P^+}{\partial x_i^+} + \delta_{i2} RaPr\theta + Pr\frac{\partial u_i^+}{\partial x_j^+ \partial x_j^+} \quad (A3)$$

A.3. Non-dimensional energy conservation equation

$$u_j^+ \frac{\partial \theta}{\partial x_j^+} = \frac{\partial^2 \theta}{\partial x_j^+ \partial x_j^+} \quad (A4)$$

The above equations are solved in conjunction with following boundary conditions:

A.4. Velocity boundary conditions

$u_1^+ = 0$ at $x_2^+ = 0$ and $x_2^+ = AR$ due to no-slip condition on horizontal walls.
$u_2^+ = 0$ at $x_2^+ = 0$ and $x_2^+ = AR$ due to impenetrability of horizontal walls.
$u_1^+ = 0$ at $x_1^+ = 0$ and $x_1^+ = 1.0$ due to impenetrability of vertical walls.
$u_2^+ = 0$ at $x_1^+ = 0$ and $x_1^+ = 1.0$ due to no-slip condition on vertical walls.

A.5. Temperature boundary conditions

$\partial\theta/\partial x_2^+ = 0$ at $x_2^+ = 0$ and $x_2^+ = AR$ due to adiabatic condition on horizontal walls.
$\theta = 1$ at $x_1^+ = 0$ at the hot vertical wall for CWT. boundary condition.
$-\partial\theta/\partial x_1^+ = 1$ at $x_1^+ = 0$ at the hot vertical wall for CWHF boundary condition.
$\theta = 0$ at $x_1^+ = 1$ at the cold vertical wall for CWT boundary condition.
$-\partial\theta/\partial x_1^+ = 1$ at $x_1^+ = 1$ at the cold vertical wall for CWHF boundary condition.

References

Bejan, A., Tien, C.L., 1978. Laminar natural convection heat transfer in a horizontal cavity with different end temperatures. J. Heat Transfer 100, 641–647.
Bejan, A., 1979. Note on Gill's solution for free convection in a vertical enclosure. J. Fluid Mech. 90, 561–568.
Bejan, A., 1980. A synthesis of analytical results for natural convection heat transfer across rectangular enclosures. Int. J. Heat Mass Transfer 23, 723–726.
Bejan, A., Al-Homoud, A.A., Imberger, J., 1981. Experimental study of high Rayleigh number convection in a horizontal cavity with different end temperatures. J. Fluid Mech. 109, 283–299.
Berkovsky, B.M., Polevikov, V.K., 1977. Numerical study of problems on high-intensive free convection. In: Spalding, D.B., Afgan, H. (Eds.), Heat transfer and turbulent buoyant convection. Hemisphere, Washington, DC, pp. 443–455.
Cormack, D.E., Leal, L.G., Imberger, J., 1974a. Natural convection in a shallow cavity with differentially heated end walls. Part 1. Asymptotic theory. J. Fluid Mech. 65, 209–229.
Cormack, D.E., Leal, L.G., Seinfeld, J.H., 1974b. Natural convection in a shallow cavity with differentially heated end walls. Part 2. Numerical solution. J. Fluid Mech. 65, 231–246.
deVahl Davis, G., 1983. Natural convection of air in a square cavity: a bench mark numerical solution. Int. J. Numer. Methods Fluids 3, 249–264.
Dong, Y., Zhai, Q., 2007. Natural convection study in an enclosure with different aspect ratios. Int. J. Mod. Phys. C 18 (12), 1903–1922.
Elder, J.W., 1965. Laminar free convection in a vertical slot. J. Fluid Mech. 23, 77–98.

Elsherbiny, S.M., Raithby, G.D., Hollands, K.G.T., 1982. Heat transfer by natural convection across vertical and inclined air layers. ASME J. Heat Transfer 104, 96–102.
Frederick, R.L., 1999. On the aspect ratio for which the heat transfer in differentially heated cavities is maximum. Int. Commun. Heat Trans. 26 (4), 549–558.
Ganguli, A.A., Pandit, A.B., Joshi, J.B., 2009. CFD simulation of heat transfer in a two-dimensional vertical enclosure. Chem. Eng. Res. Des. 87, 711–727.
Gebhart, B., Jaluria, Y., Mahajan, R.L., Sammakia, B., 1988. Buoyancy Induced Flows and Transport. Hemisphere, Washington, DC.
Gill, A.E., 1966. The boundary layer regime for convection in a rectangular cavity. J. Fluid Mech. 26, 515–536.
Imberger, J., 1974. Natural convection in a shallow cavity with differentially heated end walls. Part 3. Experimental results. J. Fluid Mech. 65, 247–260.
Lartigue, B., Lorente, S., Bourret, B., 2000. Multicellular natural convection in high aspect ratio cavity: experimental and numerical results. Int. J. Heat Mass Transfer 43, 3157–3170.
Lee, Y., Korpela, S., 1983. Multicellular natural convection in a vertical slot. J. Fluid Mech. 126, 91–124.
Le Quéré, P., 1990. A note on multiple and unsteady solutions in two-dimensional convection in a tall cavity. Trans. ASME J. Heat Transfer 112, 965–973.
Khalifa, A.J.N., 2001. Natural convective heat transfer coefficient – a review, II. Surfaces in two- and three dimensional enclosures. Energy Convers. Manage. 42, 505–517.
Newell, M.E., Schmidt, F.W., 1970. Heat transfer by laminar natural convection within rectangular enclosures. Trans. ASME C: J. Heat Transfer 92, 159–167.
Ostrach, S., 1988. Natural convection in enclosure. J. Heat Transfer 110, 1175–1190.
Patankar, S.V., 1980. Numerical Heat Transfer and Fluid Flow. Hemisphere, Washington, DC.
Roache, P.J., 1997. Quantification of uncertainty in computational fluid dynamics. Annu. Rev. Fluid Mech. 29, 123–160.
Shyy, W., Chen, M.H., 1990. Effect of Prandtl number on buoyancy-induced transport processes with and without solidification. Int. J. Heat Mass Transfer 33, 2565–2578.
Turan, O., Chakraborty, N., Poole, R.J., 2010. Laminar natural convection of Bingham fluids in a square enclosure with differentially heated side walls. J. Non-Newton. Fluid Mech. 165, 901–913.
Wakitani, S., 1996. Formation of cells in natural convection in a vertical slot at large Prandtl number. J. Fluid Mech. 314, 299–314.
Wakitani, S., 1997. Development of multicellular solutions in natural convection in an air-filled vertical cavity. Trans. ASME J. Heat Transfer 119, 97–101.
Yin, S.H., Wung, T.Y., Chen, K., 1978. Natural convection in an air layer enclosed within rectangular cavities. Int. Heat Mass Transfer 21, 307–315.
Zhao, Y., Curcija, D., Gross, W.P., 1997. Prediction of multicellular flow regime of natural convection in fenestration glazing cavities. ASHRAE Trans. 103 (1), 1–12.